Geochemistry of post-extinction microbialites as a powerful tool to assess the oxygenation of shallow marine water in the immediate aftermath of the end-Permian mass extinction

Collin P.Y.[1*], Kershaw S.[2], Tribovillard N.[3], Forel M.B.[4,5], Crasquin S.[4]

[1] Université de Bourgogne, CNRS UMR 6282 Biogéosciences, 6 Bd Gabriel, 21000 Dijon, France

[2] Institute for the Environment, Halsbury Building, Brunel University, Kingston Lane, Uxbridge, Middlesex, UB8 3PH, UK

[3] Université Lille 1, CNRS UMR 8217 Géosystèmes, bâtiment SN5, 59655 Villeneuve d'Ascq cedex, France

[4] CR2P, MNHN-CNRS-Université Pierre & Marie Curie - Paris 06, 4 place Jussieu, case 104, 75005, Paris, France

[5] Present adress: Faculty of Earth Sciences, China University of Geosciences (Wuhan), 388 Lumo Road. Wuhan, Hubei Province, China

*corresponding author: pierre-yves.collin@u-bourgogne.fr; tel: 0033(0)380396352; fax: 0033380396397

Abstract

Rapid and profound changes in Earth-surface environments and biota across the Permian-Triassic boundary are well known and relate to the end-Permian mass extinction event. This major crisis is demonstrated by abrupt facies change and the development of microbialite carbonates on the shallow marine shelves around Palaeo-Tethys and western Panthalassa. Microbialites have been described from a range of sites in end-Permian and basal Triassic

marine sedimentary rocks, immediately following the end-Permian mass extinction. Here, we present geochemical data primarily focused on microbialites. Our geochemical analysis shows that U, V, Mo and REE (Ce anomaly) may be used as robust redox proxies so that the microbialites record the chemistry of the ancient ambient sea water. Among the three trace metals reputed to be reliable redox proxies, one (V) is correlated here to terrigenous supply, the other two elements (U and Mo) do not show any significant authigenic enrichment, thereby indicating that oxic conditions prevailed during the growth of microbialites. REE profiles show a prominent negative Ce anomaly, also showing that the shallow marine waters were oxic. Our geochemical data are consistent with the presence of some benthic organisms (ostracods, scattered microgastropods, micro-brachiopods and foraminifers) in shallow marine waters that survived the mass extinction event.

Keywords

Permian-Triassic mass extinction; microbialite; Rare Earth Elements; trace elements; shallow marine water; oxygenation

Introduction

The rapid and profound changes in Earth-surface environments and biota across the Permian-Triassic boundary (PTB) are well-known and relate to the end-Permian mass extinction event. Over the past few years, these changes have become the subject of intense study using multiproxy datasets published by many authors. These datasets include: palaeontological information from many fossil groups (e.g., Erwin 2006; Brayard et al. 2009; Brayard et al. 2011), stable isotopes, principally of carbon and sulphur (Algeo et al. 2007a; Baud et al. 1989; Payne et al. 2004, Kajiwara et al. 1994; Bottrell and Newton 2006; Meyer et al. 2013), U/Th ratio (Wignall and Twitchett 2002; Algeo et al. 2007a), molecular biomarkers (Xie et al. 2005; Grice et al. 2005; Fenton et al. 2007; Luo et al. 2013), pyrite framboids (e.g. Wignall et al. 2005; Liao et al. 2010), Rare Earth Elements (REE; e.g., Ishiga et al. 1996;

Nan et al. 2002; Wright et al. 1987; Algeo et al. 2007b; Zaho et al. 2013) and modelling (Hotinski et al. 2001; Kidder and Worsley 2004; Kiehl and Shields 2005; Kump et al. 2005; Winguth & Winguth 2013). The more recent studies provide new insights into strong palaeoceanographic changes during the end-Permian mass extinction and its aftermath; the result of some of these studies is a growing opinion that oxygen levels declined in the ocean at the end-Permian and during the Early Triassic. This was proposed as an extinction mechanism and as a cause of the prolonged biotic recovery in the aftermath of the end-Permian mass extinction (e.g., Wignall and Hallam 1992; Weidlich et al. 2003 and others). The decrease of the oxygenation level in the oceans may have been caused by (1) the ocean overturn and upwelling of anoxic waters (Schoepfer et al. 2013) invading shallow shelf environments globally (Kakuwa and Matsumoto 2006; Knoll et al. 1996; Wignall and Hallam 1992), (2) the rising of the chemocline in the ocean and the spreading of the oxygen minimum zone (OMZ) on the shelves (Algeo et al. 2007a) especially in the Palaeo-Tethys Ocean which was mostly enclosed and restricted in circulation (e.g., Hotinski et al. 2001; Kiehl and Shields 2005; Kidder and Worsley 2004), (3) a rapid transgression (Wignall and Hallam 1992), (4) the expansion of the OMZ caused by an increase in nutrient flux to the oceans coupled with an intense greenhouse effect (Algeo et al. 2011; Winguth and Winguth 2013). However, the datasets also show discrepancies, because recent studies suggest that rather than a prolonged biotic recovery, the period in the aftermath of the end-Permian mass extinction is contains examples of rapid recovery (e.g., Hautmann et al. 2011) and several failed attempts of recovery (Brayard et al. 2011; Song et al. 2011). Other authors suggest that the successive aborted recoveries relate to successive shifts back to ocean anoxia (Grasby et al. 2013). However, although some data support development of prolonged anoxia, especially in the deep ocean (e.g., Kato et al. 2002; Osen et al., 2013 Luo et al., 2013), recent evidence suggests that anoxia was not a major characteristic of the shallow ocean (Forel et al. 2009; Nielsen et al. 2010; Forel et al. 2013; Proemse et al. 2013) and that

the Early Triassic was characterised by a brief oxygenation event (Bond and Wignall 2010; He et al. 2013).

Trace metals concentrations recorded in carbonate sediments are commonly used for palaeoenvironmental reconstruction through examination of redox-sensitive elements that may become enriched under low-oxygen or euxinic water conditions (e.g., Brumsack 2006; Algeo and Maynard 2004; Tribovillard et al. 2006, 2012). In the same way, REE concentrations in carbonates can be used to reconstruct the chemistry of ancient seawater masses (Wright et al. 1987; Olivier and Boyet 2006; Webb and Kamber 2000).

Here, we assess the importance of past oxygen levels in the shallow marine shelves and present geochemical data primarily derived from earliest Triassic microbialites that developed immediately following the end-Permian mass extinction, relying on earlier studies (Olivier and Boyet 2006; Webb and Kamber 2000) wherein the authors demonstrate that microbialites can be used as proxies of the chemical and palaeoenvironmental characteristic of seawater. Microbialites result largely from biologically induced carbonate precipitation (Riding, 2000); Webb and Kamber (2000) and Olivier and Boyet (2006) demonstrated that modern microbialites have shale-normalized REE patterns similar to those of modern sea water and that the trace element and REE chemistry of the microbialites faithfully records that of ancient ambient sea water. Moreover, some previous works (Banner et al. 1988) demonstrated that relative REE abundance was not changed during extensive diagenesis and REE mobilisation was only local in nature. Hence, ancient microbialites may retain their original REE patterns and trace element concentration despite relatively intense subsequent diagenesis (Kamber and Webb 2001; Olivier and Boyet 2006). In addition, Wang et al. (2005) showed that distribution patterns of REE in microbialites of Sichuan measured in coarse crystals of calcite or in adjacent micrite are similar. Also, comparison of C isotope values of carbonate between microbialite branches and adjacent micritic sediment shows that there are small but consistent variations (Mu et al. 2009).

In the present study, we demonstrate that the post-extinction microbialites incorporated REE and trace metals in equilibrium with seawater and thus that microbialites are valuable proxies for reconstructing ancient seawater chemistry. Our results suggest that the analysed shallow shelf environments were fully oxygenated in the immediate aftermath of the end-Permian extinction event. These results demonstrate the need for further high-resolution work with the same proxies to induce a comprehensive understanding of the nature of shallow shelf environments and of the palaeoceanographic changes during the latest Permian - earliest Triassic biotic crisis.

Geological setting of the study areas

The major crisis occurring through the end-Permian and early Triassic time is demonstrated by abrupt facies change associated with the End-Permian mass extinction. The carbonate platforms show drastic facies change across the Permian-Triassic (PT) event with the development of microbial carbonates, up to ten metres thick, especially in the low-palaeolatitude shallow shelf environments. Microbialites have been described from a range of sites in basal Triassic marine sedimentary rocks deposited in the immediate aftermath of the end-Permian mass extinction (e.g., Erwin 2006; Wignall and Twitchett 2002. See Kershaw et al. 2007 for the global palaeogeography with the location of the microbialite deposits).

Microbialites are defined as microbially-mediated organo-sedimentary deposits (Burne and Moore 1987). Their morphologies comprise stromatolites and thrombolites and microbial processes are the main pathway of biologically induced carbonate precipitation. Stromatolites are defined as benthic laminated organo-sedimentary deposits (Kalkowsky 1908; see Riding 2000 for a synthesis). Their morphologies are variable and include tabular, domal, columnar, dendritic or undulated laminae. Thrombolites are defined as organo-sedimentary deposits with a clotted macroscopic fabric, and are not laminated. Their morphologies encompass digitate, equant, domal or tabular forms (see Kershaw et al. 2012

for details). Hybrid stromatolites (mixtures of microbial and inorganic components; Riding 2008) are also observed in some sites (Kershaw et al. 2012).

The microbialites studied here are marine and have a widespread association with micritic sediments, indicating that they grew in relatively low-energy conditions. The micritic sediment does not contain any microbialite fragments, indicating growth of the microbialites in calm depositional environments. Uncommon coarse erosive bioclastic levels are observed in the microbialites (pers. obs; Sichuan and Guizhou) and are related to occasional currents in a normally calm depositional environment. Possible Hummocky Cross Stratifications were also observed (Kershaw et al., 2010). These sedimentary structures are interpreted as more or less distal tempestites. This is consistent with shallow shelf-seas, possibly below the fairweather wave base and above or near the stormweather wave base, in the photic zone. The post-extinction microbialites are never observed in deep shelf environments (Kershaw et al. 2012). Thus, occurrence of the microbialites relates to large scale chemical-physical changes in oceanic water but their significance as indicator of palaeoceanographic change is still under discussion.

The sites selected for this study are located in western and eastern Palaeo-Tethys and western Panthalassa (Fig. 1). In each site, microbialites occur directly on (Collin et al. 2009; Kershaw et al. 2012) or few tens of centimetres above (Baud et al. 2005; Hips and Hass 2006; Forel et al. 2013) the PT event horizon.

In western Paleo-Tethys, two sites were used to provide data in two contrasting bathymetries and sequence histories. In the Bükk Mountains of northern Hungary, a model by Hips and Haas (2006) place planar and crinkled stromatolites in an outer ramp setting, in a sequence of micritic carbonates. The conodont *Hindeodus parvus* (Kozur and Pjatakova 1976), which is recognised as the marker for the base of the Triassic (Yin et al. 1996, 2001), was found just below the microbialites (Hass et al. 2007). The stromatolites are thus dated to the early Triassic, Griesbachian, *H. parvus* zone. In contrast, in southern Turkey, shallow shelf deposits in the Antalya Nappes contain a thick and complex sequence of stromatolites,

thrombolites and hybrid microbial-inorganic structures up to a total 15 m thick (Richoz 2004; Baud et al. 2005; Kershaw et al. 2011). The Conodont *Hindeodus praeparvus* (latest Permian) is present just below the microbialites. *H. parvus* is present in the microbialite deposits which are probably of the same age as in Bükk Mountains.

The remaining two sites selected for analysis are in the South China Block, as follows. In Guizhou Province, the Great Bank of Guizhou (GBG) is an isolated shallow carbonate platform in the Nanpanjiang Basin (Lehrmann 1999) on the southern South China Block. From its palaeogeographic positioning it is interpreted as facing the Panthalassa Ocean (Fig. 1) and may therefore regarded as having a western Panthalassa position. Immediately in the aftermath of the end-Permian mass extinction, a microbialite crust (up to 14 m thick) occurred in all the GBG, marking an abrupt change in the marine environmental conditions. In the GBG, most of the microbialites are thrombolites, mainly clotted and bedded, and sometimes with a digitate fabric. In the GBG, *H. parvus* occurs within the microbialites, near the base of the sequence in some sections (Yang et al. 2011) or several tens of centimetres above the base in other sections (Lehrmann et al. 2003). The fourth site is in Sichuan Province, in the Huaying Mountains that lie on the northern side of the South China Block; the PT sedimentary rocks contained therein were facing the Paleo-Tethys Ocean during their deposition and represent the easternmost position of the Tethyan microbialites in this study. In this area, the microbialite sequences are often thinner (from 2 to 4 m thick; e.g. in the Dongwan, Laolongdong or Baizhuyuan sections) and the microbialites are thrombolites with varied morphologies (Ezaki et al. 2003, Kershaw et al. 2012). In Sichuan, the first appearance of *H. parvus* occurs several tens of centimetres above the microbialite base, suggesting that the base of microbialites is latest Permian in age (Ezaki et al. 2003, Kershaw et al. 2012).

In summary, the four selected sites illustrate four different palaeogeographic aspects; in all cases the microbialites illustrate a short period of growth (likely less than 200 kyr; Song et al., 2013). Moreover, microbialites represent one of the carbonate facies well developed

immediately in the aftermath of the end-Permian mass extinction and during the beginning of the prolonged Triassic biotic crisis. Microbialites are sediments appropriate for geochemical analysis, as demonstrated in our literature review above. Although there are numerous works on carbon isotope analysis, these deposits should receive a greater attention for measurements of other geochemical proxies, such as REE and trace metals, the subject of this study.

Material and methods

To test our methodology and as a first approach to illustrate the potential to record palaeoceanographic chemical composition of microbialites, 27 samples were selected for elemental analysis. The samples were chosen to illustrate different palaeogeographical contexts and various microbialite morphologies (stromatolites, thrombolites with domal, digitate or domal fabric) to analyse redox geochemical contents in the different settings during microbial carbonate precipitation. The samples were collected in earliest Triassic microbialites, restricted in age to the *H. parvus* zone, providing the best possible stratigraphic resolution for the studied time interval, the best possible current correlation between coeval microbialite sites (4 samples in Çürük Dag section, Turkey; 5 in Gerennavár section, Hungary; 7 in Dongwan, Laolongdong and Baizhuyuan sections in Sichuan, China; 11 in Dajiang, Dawen and Rungbao sections in Guizhou, China). Microbialites and adjacent sediment were sampled from polished slabs and each sample was finely crushed. The quality of the samples was assessed by microscopic petrographical observations, so that calcite-filled fractures or highly altered parts of rocks were excluded from sampling. For each sample, 50 mg of carbonate powder was dissolved in a mixture of concentrated HF-HNO_3. REE and trace elements were measured using a Thermofischer 2X7 series ICPMS (iSTEP, Paris 6 - Pierre and Marie Curie University – Institut de Physique du Globe de Paris). Analytical quality was checked using the CAL S standard. Analytical precision is better than 5% for all measured elements. The results are presented in Tables 1 and 2.

Results and interpretations

Trace elements as redox proxies

Many trace elements show variations in oxidation state and solubility as a function of the redox status of the depositional environment. Redox-sensitive trace metals tend to be soluble under oxidizing conditions and less soluble under reducing conditions, resulting in authigenic enrichments in oxygen-depleted sediments. Three trace metals among the most commonly used as redox proxies are uranium (U), vanadium (V) and molybdenum (Mo); see syntheses in Brumsack (2006), Tribovillard et al. (2006), and Algeo and Rowe (2012). U and V are usually authigenically enriched in sediments deposited under suboxic to anoxic conditions whereas Mo enrichment requires anoxic conditions and the presence of free sulphide ions (i.e. euxinic conditions; see discussion in Tribovillard et al. 2006, 2012; Algeo and Rowe 2012; Chappaz et al. 2014). The results are presented in Table 1.

In the present case, V is well correlated to Al (R_2 = 0.710; Fig. 2), indicating a terrigenous origin. U and Mo are poorly or not correlated to Al (R^2 = 0.436 and R^2= 0.050, respectively; Fig. 2). Concerning the Al vs. U relationship, the value of the determination coefficient R^2 suggests (from a mathematical point of view) that both elements could be correlated. However, the positive tendency drawn on Fig. 2A must be due to the two samples with the highest U and Al contents. If these two points are excluded, R^2 value falls from 0.436 down to 0.106. Consequently, the main cluster of the sample cloud does not show any tendency and the Al vs. U correlation appears to be artificial. U and Mo are also neither correlated to other terrigenous proxies (Ti, Zr, Th). As the rocks studied here are limestones, any authigenic enrichment may be masked by the very high content in carbonate. With such high carbonate content (1) a correlation between Al and U or Mo could be also masked, because Mo and U are present with very low concentrations, and (2) Al normalization (classically used to avoid dilution effect by carbonate) might be biased, because very low Al concentration causes element-to-Al ratios to be artificially high, limiting the use of

enrichment-factor calculation (see detailed discussion about Al normalization in Van der Weijden 2002 and Tribovillard et al. 2006). However, in our samples, even if detrital components (mainly clays) are present in small quantities (mean Al_2O_3 = 1.15 %; std. dev. = 0.86), their concentration is not negligible. Consequently, the calculation of enrichment factors may be attempted. Enrichment factors (EF) are calculated with X-EF = $(X/Al)_{sample}$ / $(X/Al)_{PAAS}$ where X and Al represent the weight concentrations of element X and Al, respectively, while PAAS stands for Post Archean Average Shale (Taylor and McLennan, 1985). If EF-X is larger than 1, then element X is enriched in the sample relative to its average crustal abundance. Using such enrichment factors, patterns of authigenic U-Mo covariation in marine environments provide insights regarding bottom water redox conditions (Algeo and Tribovillard 2009; Tribovillard et al. 2012). In the present sample set, all samples have low U and Mo enrichment factors (below 10 for all samples but one for U, and below 3 for all samples but 3 for Mo), indicating no or only barely detectable enrichment, but in no way a significant enrichment. In addition, when above the value 1, the enrichment factors are larger for U than for Mo. These results suggest that depositional conditions were oxic to suboxic (see discussion in Algeo and Tribovillard 2009). It is thus meant that the water column was oxygenated and that oxygen-poor, reducing, conditions developed only below the sediment-water interface. The redox-cline depth may have fluctuated below the sediment-water interface, sometimes being close to it (but still below it). In such a case, a small authigenic U enrichment (between 5 and 10) may be detected as is the case for some of the samples studied here. However it is emphasized that the redox-cline did not reach the interface nor the base of the water column (otherwise marked U- and V-, or even Mo-enrichment would have overprinted the sediment composition).

To avoid any doubt about potential biases due to Al-normalization, and hence enrichment factors calculation, another process of the analytical results is examined. In our samples (Table 1), U concentration is 0.44-1.91 ppm and Mo concentration is 0.007-0.84 ppm. Based on mean abundances in Earth's upper crust or average shale, a detrital U or Mo

concentration of 0.01-0.67 ppm and 0.00-0.34 ppm, respectively, can be expected, using the equation: $X_{detrital} = Al_{sample} \times (X/Al)_{PAAS}$. Thence, we calculated the fraction of the element concentration X_{excess}, which can be considered as resulting from authigenic enrichment, with $X_{excess} = X_{sample} - X_{detrital}$. This calculation shows that Mo_{excess} is remarkably low and not systematically observed (0.00-0.75 ppm; mean Mo_{excess} = 0.15 ppm). There is thus no detectable authigenic enrichment in Mo. U_{excess} is somewhat higher and systematically observed (0.25-1.73 ppm; mean U_{excess} = 0.85 ppm). However a ca.1 ppm-enrichment is not sufficient to conclude to any marked authigenic enrichment in U.

To sum up, among the three trace metals reputed to be reliable redox proxies, one (V) is clearly correlated to terrigenous supply, the other two elements (U and Mo) do not show significant authigenic enrichment, thereby indicating that anoxic conditions can not be detected in our dataset. When calculating trace-metal enrichment factors, a moderate authigenic-U enrichment may be observed for some samples, with no co-eval V nor Mo enrichment, which strongly suggests that both the sediment-water interface and the base of the water column kept oxygenated, even for samples recording the possible shoaling of the redox-cline within sediments.

Rare Earth Elements

REE concentration (table 2) and pattern (Fig. 3) provide a tool to assess palaeoceanographic changes of the seawater chemistry (e.g., Webb and Kamber 2000; Shields and Webb 2004; Wright et al. 1987; Négrel et al. 2006). In the present case, the clastic content is low (mean Al_2O_3 = 1.15 %; std. dev. = 0.86) and allowing the use of microbialites as a tracer of the chemical signature of sea water during the time of microbialite growth. However, the REE patterns are not flattened as should be the case if the terrigenous signal had blurred the REE signature. Thus a consistent pattern of REE emerges from all four sites (Fig. 3). The REE profiles show enrichment in the middle of the REE range, with a prominent, but variable, negative Ce anomaly. The REE profiles show a reduction in both light and heavy REE (LREE

and HREE respectively; Fig. 3). Also significant is a strong positive Eu anomaly. In order to test whether the negative Ce anomaly results from a Ce deficiency or a La relative enrichment, we draw a Pr/Pr* vs. Ce/Ce* crossplot with $Pr/Pr^* = Pr_{SN} / (0.5\ Ce_{SN} + 0.5\ Nd_{SN})$, where SN stands for "shale normalized", according to Bau and Dulski (1996). Samples with an apparent negative Ce anomaly but with Pr/Pr* close to 1 have in fact a positive La anomaly. The crossplot (Fig. 4) shows that, except for 2 (samples RUN77 and 78, stars), all samples show a true negative Ce anomaly, corresponding to a depletion of the Ce concentration in the studied samples.

Olivier and Boyet (2006) and Webb and Kamber (2000) demonstrated that microbialites may be used as proxies of palaeo-seawater chemical characteristics. These authors show that modern microbialites have shale-normalized REE patterns similar to those of modern seawater and that the trace element and REE chemistry of the microbialites faithfully records that of ancient ambient sea water. Cerium has been used as a tracer of palaeoredox conditions in marine environments. Indeed, Ce is fractionated by co-precipitation with metallic oxids or colloids under oxidizing conditions. This fractionation produces a depletion of Ce in marine seawater and in the minerals, such as calcium carbonate, which precipitate in equilibrium with seawater (as shown in modern microbialites by Webb and Kamber 2000). Conversely, under local or basinal anoxic conditions, Ce concentrations are enriched in sea-water and hence in carbonates. Here, the REE patterns exhibit shapes typical of those recorded by carbonate sediments. The REE profiles show a prominent negative Ce anomaly, except for three samples (PAJ 38, RUN 78 and B3). The Ce anomaly varies both within and between sites, yet it is almost always negative (table 2), and less than the critical value of Ce/Ce* = -0,1 (Wright et al., 1987). For the two samples on Figure 4 with a weakly pronouced Ce anomaly, only the sample RUN78 has a Ce/Ce* value higher than -0.1 ($Ce/Ce^*_{RUN78} = 0.02$). This sample also shows a weak enrichment in V (Fig. 2) but also a lower carbonate content (Table 1) in comparison with other samples of our set. So, the REE signature of this sample is difficult to interpret unequivocally. The same is true

for sample B3 but with a Ce/Ce* value lower than -0.1 (Ce/Ce^*_{B3} = -0.18). For sample RUN77, which is at the limit on the Pr/Pr* vs. Ce/Ce* crossplot (Fig. 4), the Ce/Ce* value is also at the limit value of -0.1 (Ce/Ce* = -0.1). Sample RUN77 also shows a lower carbonate content and a weak enrichment in Mo. No enrichment in V or U is observed. Thus no clear interpretation can be deduced for this sample. Overall, for all our samples, the REE signature shows that the shallow marine waters in all four sites were oxic.

Discussion

The view that the end-Permian mass extinction event was related to, and quite possibly caused by, anoxia, was given by Wignall and Hallam (1992, 1993). Later, in the literature, the role of anoxia has been reinforced (Wignall and Twittchet 2002). Successively, several processes were invoked based on anoxia and stratification of the ocean water masses (Kajiwara et al. 1994, Isozaki 1997), weak ocean circulation (Hotinski et al. 2001), euxinia and presence of free H_2S in the ocean (Wignall et al. 1998; Grice et al. 2005; Riccardi et al. 2006; Wignall et al. 2010), the presence of a euxinic photic zone (Grice et al. 2005) or an unstable chemocline overlying euxinic deep-water which periodically upwelled into the photic zone on the shelves (Riccardi et al. 2006; Algeo et al. 2007a). Even decrease of the oxygen content both in the atmosphere and ocean was mentioned (Weidlich et al. 2003). These studies used various approaches and showed that anoxia, or even occasional euxinia, can be admitted for basinal deposits. For the shelves, some works used the presence of pyrite framboids, to suggest the occurrence of anoxia (e.g. Wignall et al. 2005; Liao et al. 2010). However pyrite framboids may be abundant in sedimentary settings such as the one described here, with oxygen-restricted conditions being present only below the sediment-water interface (see discussions in Tribovillard et al., 2008; Bond and Wignall, 2010; Rickard, 2012). Moreover, the ostracod distribution suggests that shelf environments were well oxygenated in several shelf localities around the Tethys or on the Panthalassa margin (Forel

et al. 2009, 2013). Finally, few studies have focused on shallow shelf environments (Dolenec et al. 2001; Algeo et al. 2007a), where the role of anoxia is uncertain or occasional.

As noted earlier, immediately in the aftermath of the end-Permian mass extinction, and during the beginning of the biotic crisis which has continued for several million years, the well-developed Upper Permian bioclastic carbonate platforms are replaced by prokaryote-dominated carbonated biocontructions (microbialites) during the earliest Triassic (Kershaw et al. 2012). These carbonate sequences provide high-resolution archives of shallow marine environmental changes (Weidlich and Bernecker 2007). Trace-element abundances in sedimentary deposits allow reconstruction of the physico-chemical conditions that prevailed during the deposition of sediments or the precipitation of carbonates. More specifically, redox sensitive trace metals (U, V, Mo), and their potential authigenic enrichment in the sediments, are useful palaeoredox proxies (e.g., Algeo and Maynard 2004; Brumsack 2006; Tribovillard et al. 2006; Algeo and Tribovillard 2009; Algeo and Rowe 2012; Tribovillard et al. 2012 for detailed processes of enrichment). For example, in the case of U and V enrichment without co-eval Mo enrichment, suboxic or anoxic depositional without free H_2S can be inferred. Conversely, sediments exhibiting concurrent enrichments in U, V and Mo reflect euxinic conditions at the sediment interface or higher up in the water column. Here, the studied rocks do not record any enrichment in redox sensitive trace metals (U and Mo, Fig. 5; and V), which indicates that shelf depositional conditions were neither durably suboxic, nor anoxic, nor even euxinic during the microbialite growth. The REE patterns show also typical shapes of oxygenated marine environments.

Finally, in our four sites, the post-extinction microbialites contain a very good record of geochemical change, faithfully recording trace element and REE chemistry of the ancient ambient sea water. Our results indicate that the marine shelf environments studied here were oxic in the aftermath of the end-Permian mass extinction and at the beginning of the biotic crisis, during the early Triassic (*H. parvus* conodonte zone). Anoxia or euxinia occurred in the deep ocean, as shown by several authors (e.g., Kajiwara et al. 1994; Ishiga et al. 1996;

Kakuwa 2008; Algeo et al. 2010); and in deep shelf environments (e.g., Grice et al. 2005; Wignall et al. 2005). However, if upwelling of anoxic waters contributed to the biodiversity crisis, as suggested by e.g., Algeo et al. (2007a), anoxic waters did not extend through the entire water column, and in particular, they did not undergo large scale invasion of the shallow shelf environment. Under these circumstances, the role of euxinia on the shallow marine shelf represented by the localities studied here is discarded. Moreover, there are numerous groups of oxygen-demanding benthic organisms in shallow marine fossil records throughout the earliest Triassic microbialites in all the sites studied (Forel et al. 2013). Our geochemical data are consistent with the presence of numerous groups of benthic organisms in shallow marine waters throughout the boundary sequence that survived the mass extinction event, and are therefore primary evidence that oxic conditions prevailed in shallow marine waters. In particular, ostracod palaeobiology does not record any drop in oxygenation in some sites, assuming Permo-Triassic ostracods had the same physiology as that of modern ones (Forel et al., 2013). These results agree with the conclusions of Song et al. (2013) who interpreted a pulse of anoxia linked with the mass extinction just before the microbialites growth, which then occur in a re-oxygenated interval before a second pulse of anoxia.

Thus, if anoxia contributed to, or even caused, the decrease of the biodiversity in the deep ocean environment, our results dispute other research, referred to in this paper, which interprets anoxia in shallow marine environments immediately in the aftermath of the end-Permian mass extinction and during the beginning of the prolonged Triassic biotic crisis. Thus interpretations of anoxia in these shallow marine sediments must be reconsidered, and that a multi causal origin of the event may be envisioned.

Conclusion

Our geochemical investigations were conducted on four different geographic locations across Tethys and western Panthalassa, in carbonate microbialites, which grew during the early

Triassic (*H. parvus* conodonte zone) on shallow marine shelves in the aftermath of the end-Permian extinction and during early Triassic, at the beginning of the biotic crisis. This work shows that microbialites are valuable proxies for reconstructing ancient seawater chemistry. Among the three trace metals reputed to be reliable redox proxies, in our samples, V is correlated to terrigenous supply, but U and Mo do not show any authigenic enrichment, demonstrating they do not indicate anoxia. The REE patterns of the studied samples exhibit shapes typical of those recorded by carbonate precipitated in marine environments and show a prominent negative Ce anomaly characteristic of precipitation of carbonate in an oxic environment. In the present study, the post-extinction microbialites incorporated REE and trace metals in equilibrium with seawater and we interpret our results to indicate that the shallow shelf environments were fully oxygenated in the immediate aftermath of the end-Permian extinction.

Acknowledgments

We are grateful to A. Lethiers, F. Delbès, A. Michel and B. Villemant for technical support. The authors thank Q. Feng, J. Haas, K. Hips and Erdal Kosun for their help in the field. This paper is a contribution to IGCP 572 “Restoration of marine ecosystems following the Permian-Triassic mass extinction: lessons for the present”. K. Föllmi and an anonymous reviewer are thanked for their constructive suggestions that helped to improve the manuscript.

REFERENCES :

Algeo TJ, Rowe H (2012) Paleoceanographic applications of trace-metal concentration data. Chemical Geology 324–325: 6-18.

Algeo TJ, Ellwood B, Thi K, Nguyen T, Rowe H, Maynard B (2007a) The Permian-Triassic boundary at Nhi Tao, Vietnam: evidence for recurrent influx of sulfidic watermasses to a shallow-marine carbonate platform. Palaeogeography, Palaeoclimatology, Palaoecology 252: 304-327.

Algeo TJ, Hannigan R, Rowe H, Brookfield M, Baud A, Krystyn L, Ellwood B (2007b) Sequencing events across the Permian-Triassic boundary, Guryul Ravine (Kashmir, India). Palaeogeography, Palaeoclimatology, Palaoecology 252: 328-346.

Algeo TJ, Hinnov L, Moser J, Maynard JB, Elswick E, Kuwahara K, Sano H (2010) Changes in productivity and redox conditions in the Panthalassic Ocean during the latest Permian. Geology 38: 187-190.

Algeo TJ, Kuwahara JB, Sano H, Bates S, Lyons T, Elswick E, Hinnov L, Ellwood B, Moser J, Maynrad JB (2011) Spatial variation in sediment fluxes, redox conditions, and productivity in the Permian-triassic Panthalassic Ocean. Palaeogeography, Palaeoclimatology, Palaoecology 308: 65-83.

Algeo TJ, Maynard JB (2004) Trace-element behavior and redox facies in core shales in Upper Pennsylvanian Kansas-type cyclothems. Chemical Geology 206: 289-318.

Algeo TJ, Tribovillard N (2009) Environmental analysis of paleoceanographic systems based on molybdenum-uranium covariation. Chemical Geology 268: 211-225.

Banner JL, Hanson GN, Meyers WJ (1988) Rare earth elements and Nd isotopic variations in regionally extensive dolomites from Burlington-Keokuk formation (Mississipian): Implications for REE mobility during carbonate diagenesis. Journal of Sedimentary Petrology 58: 415-432.

Bau M, Dulski P (1996) Distribution of yttrium and rare earth elements in the Penge and Kuruman iron-formations, Transvaal Supergroup. South-Africa. Precambrian Research 79: 37-55.

Baud A, Richoz S, Marcoux J (2005) Calcimicrobial cap rocks from the basal Triassic units: western Taurus occurrences (SW Turkey). C. R. Palevol 4: 569-582.

Baud A, Holser WT, Magaritz M (1989) Permian-Triassic of the Tethys : carbon isotopes studies. Geologische Rundschau 78: 649-677.

Bond DPG, Wignall PB (2010) Pyrite framboids study of marine Permian-Triassic boundary sections: a complex anoxic event and its relationship to contemporaneous mass extinction. GSA Bulletin 122: 1265-1279.

Bottrell SH, Newton RJ (2006) Reconstruction of changes in the global sulphur cycling from marine sulphate isotopes. Earth Sci. Rev. 75: 59-83.

Brayard A, Escarguel G, Bucher H, Monnet C, Brühwiler T, Goudemand N, Galfetti T, Guex J (2009) Good genes and good luck: ammonoid diversity and the end-Permian mass extinction. Science, 325: 1118-1121.

Brayard A, Vennin E, Olivier N, Bylund KG, Jenks J, Stephen DA**,** Bucher H, Hofmann R, Goudemand N, Escarguel G (2011) Transient metazoan reefs in the aftermath of the end-Permian mass extinction. Nature Geoscience 4: 693-697.

Brumsack HJ (2006) The trace metal content of recent organic carbon-rich sediments: Implications for Cretaceous black shale formation. Palaeogeography, Palaeoclimatology, Palaoecology 232: 344-361.

Burne RV, Moore LS (1987) Microbialites: organosedimentary deposits of benthic microbial communities. Palaios 2: 241-254.

Chappaz A, Lyons TW, Gregory DD, Reinhard CT, Gill BC, Li C, Large RR (2014) Does pyrite act as an important host for molybdenum in modern and ancient euxinic sediments? Geochimica et Cosmochimica Acta 126: 112–122.

Collin PY, Kershaw S, Crasquin-Soleau S, Feng Q (2009) Facies changes across the Permian-Triassic boundary event horizon, Great Bank of Guizhou, South China: a controversy of erosion and dissolution. Sedimentology 56: 677-693.

Dolenec T, Lojen S, Ramovs A (2001) The Permian-Triassic boundary in Western Slovenia (Idrijca Valley section): magnetostratigraphy, stable isotopes, and elemental variations. variations. Chemical Geology 175: 175-190.

Erwin DH (2006) Extinction: How life on Earth Nearly Died 250 Million Years Ago. Princeton Univ. Press, Princeton, New Jersey.

Ezaki Y, Liu J, Adachi N (2003) Earliest Triassic microbialite micro- to megastructures in the Huaying area of Sichuan Province, south China: implications for the nature of oceanic conditions after the end-Permian extinction. Palaios 18: 388-402.

Fenton S, Grice K, Twitchett RJ, Böttcher ME, Looy CV, Nabbefeld B (2007) Changes in biomarker abundances and sulfur isotopes of pyrite across the Permian-Triassic (P/Tr) Schuchert Dal section (East Greenland). Earth and Planetary Science Letters 262: 230-239.

Forel MB, Crasquin S, Kershaw S, Feng Q, Collin PY (2009) Early Triassic ostracods (Crustacea) associated with microbialites in South China. Australian J. of Earth Sc. 56: 815-823.

Forel MB, Crasquin S, Kershaw S, Collin PY (2013). In the aftermath of the end-Permian extinction: the microbialite refuge. Terra Nova 25: 137-143.

Golonka J (2002) Plate-tectonic maps of the Phanerozoic, in: Kiessling, W., Flügel, E., Golonka, J. (Eds.), Phanerozoic Reef Patterns. SEPM Spec. Publ. 72: 21–76.

Grasby SE, Sanei H, Beauchamp B, Chen ZH (2013). Mercury deposition through the Permo-Triassic Biotic Crisis. Chemical Geology 351: 209-216.

Grice K, Cao C, Love GD, Böttcher ME, Twitchett RJ, Grosjean E, Summons RE, Turgeon SC, Dunning W, Jin Y (2005) Photic zone euxinia during the Permian-Triassic superanoxic event. Science 307: 706-709.

Haas J, Demény A, Hips K, Zajzon N, Weiszburg T, Sudar M Pálfy J (2007) Biotic and environmental changes in the Permian–Triassic boundary interval recorded on a western Tethyan ramp in the Bükk Mountains, Hungary. Global and Planetary Change 55: 136–154.

Hautmann M, Bucher H, Brühwiler T, Goudemand T, Kaim A, Nützel A (2011) An unusually diverse mollusc fauna from the earliest Triassic of South China and its implications for benthic recovery after the end-Permian biotic crisis. Geobios 44: 71-85.

He L, Wang Y, Woods A, Li G, Yang H, Liao W (2013) An oxygenation event occured in deep shelf settings immediately after the end-Permian mass extinction in South China. Global and Planetary Change 101: 72-81.

Hips K, Haas J (2006) Calcimicrobial stromatolites at the Permian-Triassic boundary in a western Tethyan section, Bükk, Hungary. Sed. Geol. 185: 239-253.

Hotinski RM, Bice KL, Kump LR, Najjar RG, Arthur MA (2001) Ocean stagnation and end-Permian anoxia. Geology 29: 7-10.

Ishiga H, Ishida K, Dozen K, Musashino M (1996) Geochemical characteristic of pelagic chert sequences across the permian-Triassic boundary in southwest Japan. The Island Arc 5: 180-193.

Isozaki Y (1997) Permo-Triassic superanoxia and stratified superocean: records from the lost deep sea. Science 276: 235-238.

Kajiwara Y, Yamakita S, Ishida K, Ishiga H, Imai A (1994) Development of a largely anoxic stratified ocean and its temporary massive mixing at the Permian/Triassic boundary supported by the sulfur isotopic record. Palaeogeography, Palaeoclimatology, Palaoecology 111: 367-379.

Kakuwa Y (2008) Evaluation of palaeo-oxygenation of the ocean bottom across the Permian-triassic boundary. Global and Planetary Change 63: 40-56.

Kakuwa Y, Matsumoto R (2006) Cerium negative anomaly just before the Permian and Triassic boundary event - the upward expansion of anoxia in the water column. Palaeogeography, Palaeoclimatology, Palaoecology 229: 335-344.

Kalkowsky E (1908) Oolith und Stromatolith im norddeutschen Buntsandstein. Zeitschr. Deutsc. geol. Gesellsch. 60: 68-125.

Kamber BS, Webb G (2001) The geochemistry of late Archean microbial carbonate: Implications for ocean chemistry and continental erosion history. Geochim. Cosmochim. Acta 65: 2509-2525.

Kato Y, Nakao K, Isozaki Y (2002) Geochemistry of Late Permian to Early Triassic pelagic chert from southwest Japan: implications for an oceanic redox change. Chemical Geology 182: 15-34.

Kershaw S, Li Y, Crasquin-Soleau S, Feng Q, Mu X, Collin PY, Reynolds A, Guo L (2007) Earliest Triassic microbialites in the South China Block and other areas; controls on their growth and distribution. Facies 53: 409-425.

Kershaw S, Crasquin S, Forel MB, Randon C, Collin PY, Kosun E, Richoz S, Baud A (2011) Earliest Triassic microbialites in Cürük Dag, southern Turkey : composition, sequences and controls on formation. Sedimentology 58: 739-755.

Kershaw S, Crasquin S, Li Y, Collin PY, Forel MB, Mu X, Baud A, Wang Y, Xie S, Maurer F, Guo L (2012) Microbialites and global environmental change across the Permian-Triassic boundary: a synthesis. Geobiology 10: 25-47.

Kidder DL, Worsley TR (2004) Causes and consequences of extreme Permo-Triassic warming to globally equable climate and relation to the Permo-Triassic extinction and recovery. Palaeogeography, Palaeoclimatology, Palaoecology 203: 207-237.

Kiehl JT, Shields CA (2005) Climate simulation of the latest 382 Permian: implications for mass extinction. Geology 33: 757-760.

Knoll AH, Bambach RK, Canfield DE, Grotzinger JP (1996) Comparative Earth history and Late Permian mass extinction. Science 273: 452-457.

Kozur H, Pjatakova M (1976) Die Conodontenart *Anchignathodus parvis* n. sp. eine wichtige Leitform der basalen Trias. Proceedings of the Koninklijke Nederlandse Academie van Wetenschappen. Series B: Physical Sciences 79: 123–128.

Kump LR, Pavlov A, Arthur MA (2005) Massive release of hydrogen sulfid to the surface ocean and atmosphere during intervals of oceanic anoxia. Geology 33: 397-400.

Lehrmann DJ (1999) Early Triassic calcimicrobial mounds and biostromes of the Nanpanjiang Basin, South China. Geology 27: 359-362.

Lehrmann DL (1999) Early Triassic calcimicrobial mounds and biostromes of the Nanpanjiang Basin, South China. Geology 27: 359-362.

Lehrmann DL, Payne JL, Felix SV, Dillett PM, Wang H, Yu Y, Wei J (2003) Permian-Triassic boundary sections from shallow-marine carbonate platforms of the Nanpanjiang Basin, south China: Implications for oceanic conditions associated with the end-Permian extinction and its aftermath. Palaios 18: 138-152.

Liao W, Yang W, Kershaw S, Weng Z, Yang H (2010) Shallow-marine dysoxia across the Permian-Triassic boundary: evidence fron pyrite framboids in the microbialites in South China. Sedimentary Geology 232: 77-83.

Luo G, Wang Y, Grice K, Kershaw S, Ruan X, Algeo TJ, Yang H, Jia C, Xie S (2013) Microbial-algal community changes during the latest Permian ecological crisis: evidence from lipid biomarkers at Cili, South China. Global and Planetary Change 105: 36-51.

Meyer KM, Yu M, Lehrmann D, Van de Schootbrugge B, Payne JL (2013) Constraints on Early Triassic carbon cycle dynamics from paired organic and inorganic carbon isotope records. Earth and Planetary Science Letters 361: 429-435.

Mu X, Kershaw S, Li Y, Guo L, Qi Y, Reynolds A (2009) High-resolution carbon isotope changes in the Permian–Triassic boundary interval, Chongqing, South China; implications for control and growth of earliest Triassic microbialites. J. of Asian Earth Sc. 36: 434-441.

Nan J, Congqiang L, Dequan Z, Zhuming W (2002) REE geochemical study of the Permian-Triassic marine sedimentary environment in Guizhou Province. Chinese J. of Geochem. 21: 348-361.

Négrel P, Casanova J, Bruhlet J (2006) REE and Nd isotope stratigraphy of the Late Jurassic carbonate platform, eastern Paris Basin, France. Journal of Sedimentary Research 76: 605-617.

Nielsen JK, Shen Y, Piasecki S, Stemmerik L (2010) No abrupt change in redox condition caused the end-Permian marine ecosystem collapse in the East Greenland Basin. Earth and Planet. Sci. Letters 291: 32-38.

Olivier N, Boyet M (2006) Rare-earth and trace elements of microbialites in Upper Jurassic coral- and sponge-microbialite reefs. Chemical Geology 230: 105-123.

Osen A, Winguth AME, Winguth C, Scotese CR (2013) Sensitivity of the Late Permian climate to bathymetric features and implications for the mass extinction. Global and Planetary Change 105: 170-178.

Proemse BC, Grasby SE, Wieser ME, Mayer B, Beauchamp B (2013) Molybdenum isotopic evidence for oxic marine conditions during the latest Permian extinction. Geology 41: 967-970.

Payne JL, Lehrmann DJ, Wei J, Orchard MJ, Schrag DP, Knoll AH (2004) Large perturbations of the carbon cycle during recovery from the end-Permian extinction. Science 305: 506-509.

Riccardi AL, Arthur LA, Kump LR (2006) Sulfur isotopic evidence for chemocline upward excursion during the end-Permian mass extinction. Geochimica Cosmochimica Acta 70: 5740-5752.

Rickard D (2012) Sulfidic sediments and sedimentary rock. Developments in Sedimentology 65, Elsevier, 801 p.

Riding R (2000) Microbial carbonates: the geological record of calcified bacterial-algal mats and biofilms. Sedimentology 47: 179-214.

Riding R (2008) A biogenic, microbial and hybrid authigenic carbonate crusts: components of Precambrian stromatolites. Geologia Croatia 61: 73-103.

Richoz S (2004) Stratigraphie et variations isotopique du carbone dans le Permien supérieur et le Trias inférieur de la Néotéthys (Turquie, Oman et Iran). PhD Thesis, Lausanne University, Switzerland.

Schoepfler SD, Henderson CM, Garrison GH, Ward PD, Foriel J, Selby D, Hower JC, Algeo TJ, Shen Y (2013) Termination of a continental-margin up-welling system at the Permian-Triassic boundary (Opal Creek, Alberta, Canada). Global and Planetary Change 105: 21-35.

Shields GA, Webb GE (2004) Has the REE composition of seawater changed over geological time? Chemical Geology 204: 103-107.

Song HG, Wignall PB, Chen ZQ, Tong JN, Bond DPG, Lai XL, Zhao XM, Jiang HS, Yan CB, Nin ZJ, Chen J, Yang H, Wang YB (2011) Recovery tempo and pattern of marine ecosystems after the end-Permian mass extinction. Geology 39: 739-742.

Song H, Wignall PB, Tong J, Yin H (2013) Two pulses of extinction during the Permian-Triassic crisis. Nature Geoscience 6: 52-56.

Taylor SR, McLennan SM (1985) The Continental Crust: Its Composition and Evolution. Blackwell, Oxford.

Tribovillard N, Algeo TJ, Lyons TW, Riboulleau A (2006) Trace metals as paleoredox and paleoproductivity proxies: An update. Chemical Geology 232: 12-32.

Tribovillard N, Lyons TW, Riboulleau A, Bout-Roumazeilles V (2008) A possible capture of molybdenum during early diagenesis of dysoxic sediments. Bull. Soc. Geol. Fr. 179: 3-12.

Tribovillard N, Algeo TJ, Baudin F, Riboulleau A (2012). Analysis of marine environmental conditions based on molybdenum-uranium covariation - Applications to Mesozoic paleoceanography. Chemical Geology 324-325: 46-58.

Van der Weijden CH (2002) Pitfalls of normalization of marine geochemical data using a common divisor. Marine Geology 184: 167-187.

Wang Y, Tong J, Wang J, Zhou X. (2005) Calcimicrobialite after end-Permian mass extinction in South China and its palaeoenvironmental significance. Chinese Science Bull. 50: 665-671.

Webb G, Kamber BS (2000) Rare earth elements in Holocene 432 reefal microbialites: A new shallow seawater proxy. Geochim. Cosmochim. Acta 64: 1557-1565.

Weidlich O, Bernecker M (2007) Differential severity of Permian-Triassic environmental changes on Tethyan shallow-water carbonate platforms. Global and Planetary Change 55: 209-235.

Weidlich O, Kiessling W, Flügel E (2003) Permian-Triassic boundary interval as a model for forcing marine ecosystem collapse by long-term atmospheric oxygen drop. Geology 31: 961-964.

Wignall PB, Hallam A (1992) Anoxia as a cause of the Permian/Triassic mass extinction: facies evidence from northern Italy and the western United States. Palaeogeography, Palaeoclimatology, Palaoecology 93: 21-46.

Wignall PB, Hallam A (1993) Griesbachian (earliest Triassic) palaeoenvironmental changes in the Salt Range, Pakistan and southern China and their bearing on the Permo-Triassic mass extinction. Palaeogeography, Palaeoclimatology, Palaoecology 102, 215-237.

Wignall PB, Morante R, Newton R (1998) The Permo-Triassic transition in Spitsbergen: $\delta^{13}C_{org}$ chemostratigraphy, fe and S geochemistry, facies, fauna and trace fossils. Geological Magazine 135: 47-62.

Wignall PB, Bond DPG, Kuwahara K, Kakuwa Y, Newton RJ, Poulton SW (2010) An 80 million year oceanic redox history from Permian to Jurassic pelagic sediments of the Mino-Temba terrane, SW Japan, and the origin of four mass extinctions. Global and Planetary Change 71: 109-123.

Wignall PB, Newton R, Brookfield ME (2005) Pyrite framboid evidence for oxygen poor deposition during the Permian-Triassic crisis in Kashmir. Palaeogeography, Palaeoclimatology, Palaoecology 216: 183-188.

Wignall PB, Twitchett RJ (2002) Extent, duration and nature of the Permian-Triassic superanoxic event. Geol. Soc. America Spec. Publ. 356: 395-413.

Winguth AME, Winguth C (2013) Precession-driven monsoon variability at the Permian-Triassic boundary - implications for anoxia and the mass extinction. Global and Planetary Change 105: 159-169.

Wright J, Schrader H, Holser WT (1987) Paleoredox variations in ancient oceans recorded by rare earth elements in fossil apatite. Geochim. Cosmochim. Acta 51: 631-644.

Xie S, Pancost RD, Yin H, Wang H, Evershad RP (2005) Two episodes of microbial change coupled with Permo/Triassic faunal mass extinction. Nature 434: 494-497.

Yang H, Chen ZQ, Wang Y, Tong J, Song H, Chen J (2011) Composition and structure of microbialite ecosystems following the end-Permian mass extinction in South China. Palaeogeography, Palaeoclimatology, Palaeoecology 308: 111-128.

Yin H, Wu S, Ding M, Zhang K, Tong J, Yang F, Lai X (1996) The Meishan section, candidate of the Global Stratotype Section and Point of Permian–Triassic boundary. *In*: H.F Yin (ed.), The Paleozoic–Mesozoic Boundary Candidates of the Global Stratotype Section and Point of the Permian–Triassic Boundary, 31–48. China University of Geosciences Press, Wuhan.

Yin H, Zhang K, Tong J, Yang Z, Wu S (2001) The global stratotype section and point of the Permian–Triassic boundary (GSSP). Episodes 24: 102–114.

Zaho L, Chen ZQ, Algeo TJ, Chen JP, Chen YL, Tong JN, Gao S, Zhou L, Hu Z, Liu YS (2013) Rare-earth element patterns in conodont albid crowns: Evidence for massive inputs of volcanic ash during the latest Permian biocrisis? Global and Planetary Change 105: 135-150.

Figure captions

Fig. 1. Palaeogeographic map of the Permian-Triassic boundary time interval (modified from Golonka 2002) showing locations of the four sample sites in this study (1 - China, Guizhou; 2 - China, Sichuan; 3 - Hungary; 4 - Turkey).

Fig. 2. Crossplots illustrating the significant correlations linking Al to V, indicating that V trace is strongly linked to the detrital supply. U and Mo are poorly correlated to Al (R^2 = 0.436 and R^2= 0.050, respectively).

Fig. 3. Shale-normalised REE patterns for microbialites from Turkey, Hungary and China (Sichuan and Guizhou).

Fig. 4. Crossplot illustrating the relations between Cerium and Praseodymium anomalies. The diagram is used to determine whether a Ce anomaly is due to a lack of Ce (true Ce anomaly) or an excess of Lanthanum. Here all samples but three deviate from the Pr/Pr* = 1 line, indicating a true Ce anomaly.

Fig. 5. Mo_{EF} versus U_{EF} for microbialites. solid lines show Mo/U molar ratio equal to the seawater value (1xSW) and to fractions thereof (0.3XSW, 0.1xSW).

Tables

Table 1. The major elements and trace elements distributions of the microbialites. Major elements contents are expressed in weight percents (wt %). $CaCO_3$ values are calculated from the CaO content, as if Ca were only present in the form of carbonate. Trace elements are expressed in ppm or µg/g, EF stands for enrichment factors, xs stands for "excess", that

is, the portion of the concentration in excess to what could be expected, basing on average crustal concentrations (see text for explanations). CS/Do: China, Sichuan province, Dongwan section; CS/B: China, Sichuan, Baizhuyuan section; CS/L: China, Sichuan, Laolongdong section; CG/Daw: China, Guizhou province, Dawen section; CG/Daj: China, Guizhou province, Dajiang section; CG/R: China, Guizhou province, Rungbao section; H/G: Hungary, Gerennavar section; T/CD; Turkey, Çürük Dag section.

Table 2. REE distributions of the microbialites. REE are given as raw, non-normalized data. CS/Do: China, Sichuan province, Dongwan section; CS/B: China, Sichuan, Baizhuyuan section; CS/L: China, Sichuan, Laolongdong section; CG/Daw: China, Guizhou province, Dawen section; CG/Daj: China, Guizhou province, Dajiang section; CG/R: China, Guizhou province, Rungbao section; H/G: Hungary, Gerenovar section; T/CD; Turkey, Çürük Dag section.

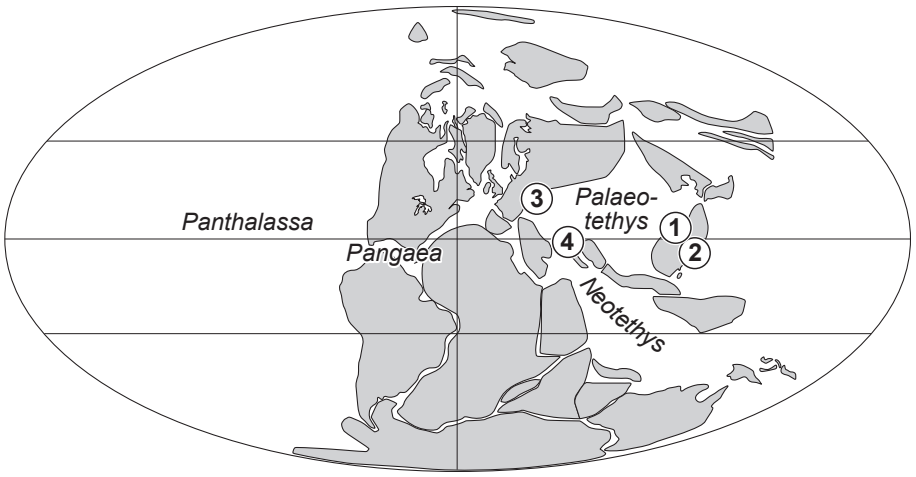
Panthalassa
Pangaea
Palaeo-
tethys
Neotethys
1
2
3
4

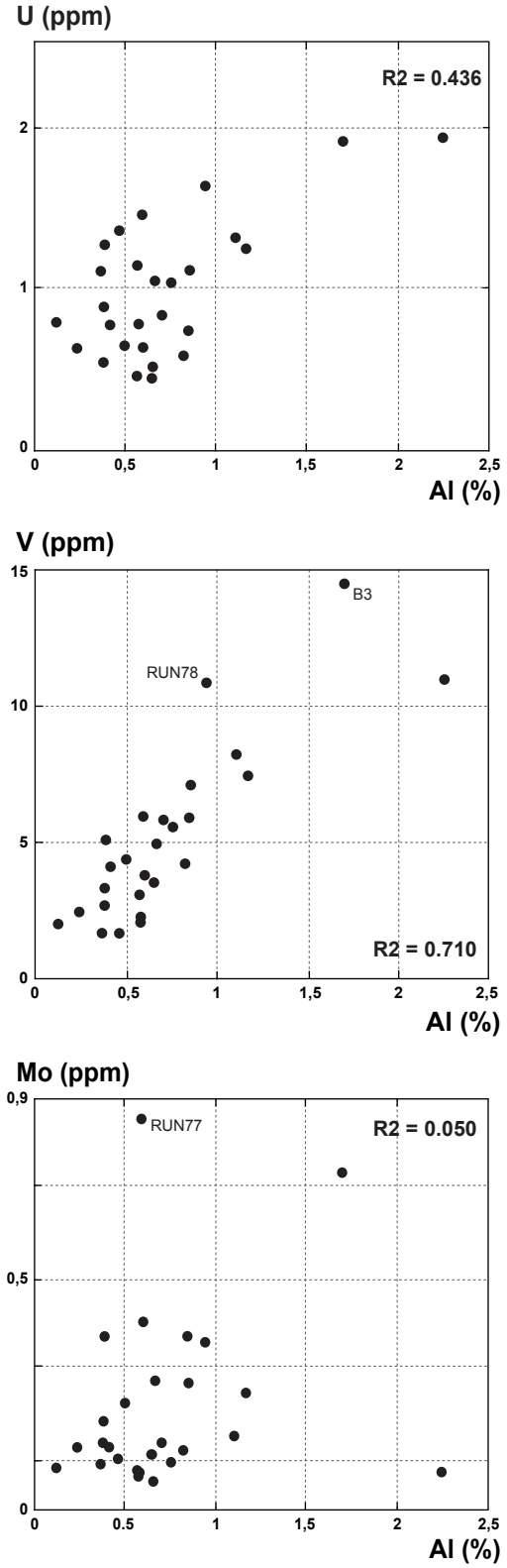
U (ppm)
R2 = 0.436
0
1
2
0
0,5
1
1,5
2
2,5
Al (%)
V (ppm)
B3
RUN78
R2 = 0.710
0
5
10
15
0
0,5
1
1,5
2
2,5
Al (%)
Mo (ppm)
RUN77
R2 = 0.050
0
0,5
0,9
0
0.5
1
1,5
2
2,5
Al (%)

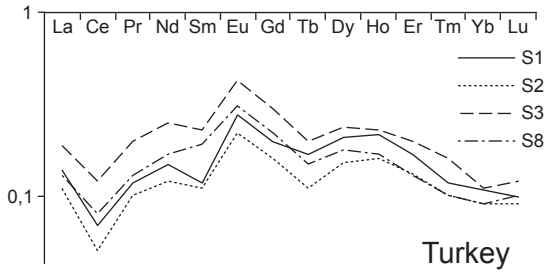
1
0,1
La Ce Pr Nd Sm Eu Gd Tb Dy Ho Er Tm Yb Lu
S1
S2
S3
S8
Turkey

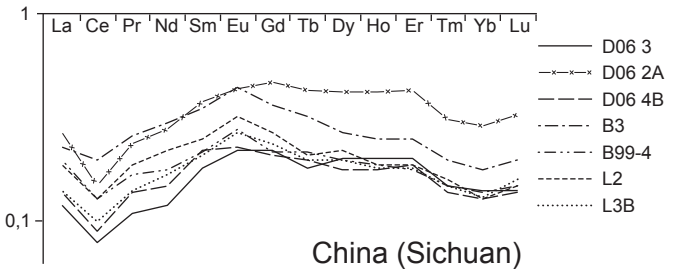
1
0,1
La Ce Pr Nd Sm Eu Gd Tb Dy Ho Er Tm Yb Lu
D06 3
D06 2A
D06 4B
B3
B99-4
L2
L3B
China (Sichuan)

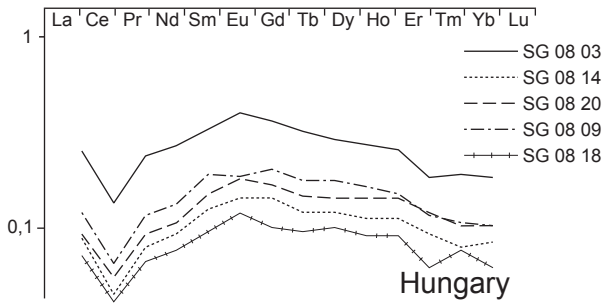
1
0,1
La Ce Pr Nd Sm Eu Gd Tb Dy Ho Er Tm Yb Lu
SG 08 03
SG 08 14
SG 08 20
SG 08 09
SG 08 18
Hungary

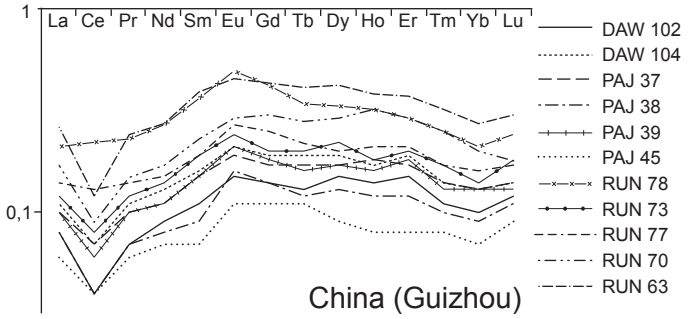
1
0,1
La Ce Pr Nd Sm Eu Gd Tb Dy Ho Er Tm Yb Lu
DAW 102
DAW 104
PAJ 37
PAJ 38
PAJ 39
PAJ 45
RUN 78
RUN 73
RUN 77
RUN 70
RUN 63
China (Guizhou)

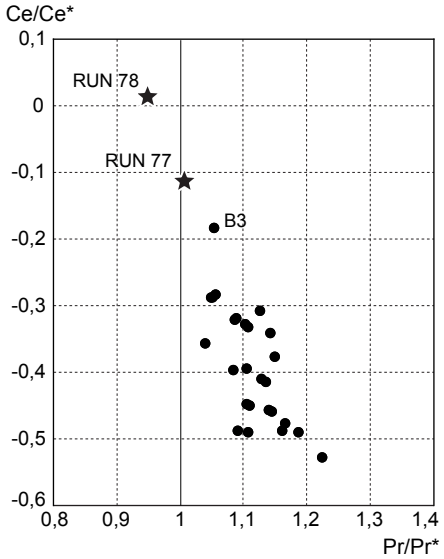
Ce/Ce*
0,1
0
-0,1
-0,2
-0,3
-0,4
-0,5
-0,6
RUN 78
RUN 77
B3
0,8
0,9
1
1,1
1,2
1,3
1,4
Pr/Pr*

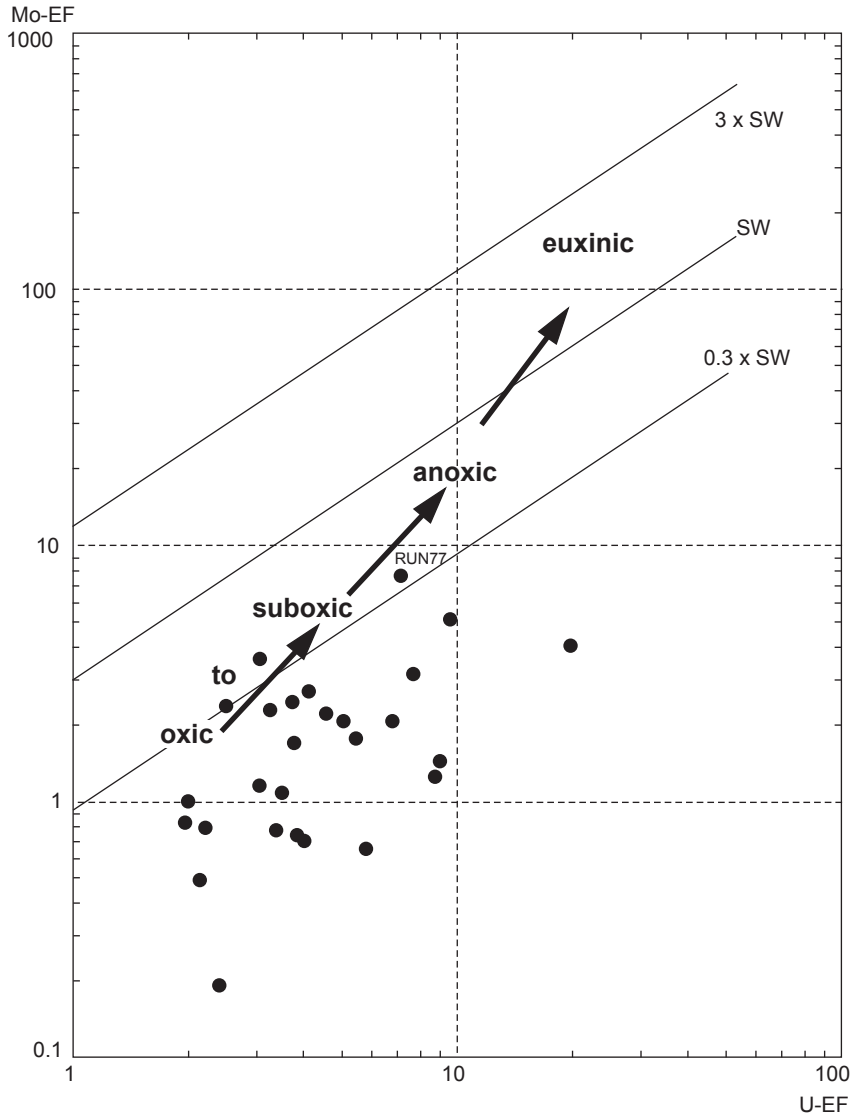
Mo-EF
1000
100
10
1
0.1
1
10
100
U-EF
3 x SW
SW
0.3 x SW
euxinic
anoxic
suboxic
to
oxic
RUN77

Locations / sections	Samples	Al_2O_3 (wt %)	Fe_2O_3 (wt %)	MnO (wt %)	TiO_2 (wt %)	K_2O (wt %)	MgO (wt %)	CaO (wt %)	$CaCO_3$ (wt %)	Na_2O (wt %)	Th (ppm)	U (ppm)	V (ppm)	Cr (ppm)	Co (ppm)	Ni (ppm)	Cu (ppm)	Zn (ppm)	Sr (ppm)	Zr (ppm)	Mo (ppm)	Cd (ppm)	Sb (ppm)	Ba (ppm)	Al (wt %)	U-EF	Mo-EF	U xs (ppm)	Mo xs (ppm)
CS/Do	DO6 4B	1,13	0,08	0,17	0,01	0,07	2,96	48,87	81,45	0,02	0,55	0,63	3,82	7,79	1,29	8,54	6,76	13,43	552,60	5,52	0,41	0,08	0,098	21,75	0,60	3,0	3,6	0,4	0,3
	DO6 3	0,71	0,07	0,10	0,01	0,05	0,79	52,07	86,79	0,02	0,39	0,54	2,71	7,23	1,00	9,15	10,95	11,82	765,12	4,18	0,19	0,09	0,193	15,29	0,38	4,1	2,7	0,4	0,1
	DO6 2A	2,20	0,09	0,04	0,01	0,12	0,77	48,23	80,38	0,03	1,08	1,24	7,51	12,11	1,62	12,95	11,76	28,38	614,75	9,95	0,25	0,29	0,320	42,89	1,16	3,1	1,2	0,8	0,0
CS/B	B 3	3,20	0,15	0,06	0,03	0,18	6,36	35,39	58,98	0,05	1,91	1,91	14,65	24,91	3,15	33,95	24,88	21,40	478,22	27,85	0,73	0,25	0,577	55,96	1,70	3,2	2,3	1,3	0,4
	B 99-4	1,59	0,10	0,02	0,01	0,10	1,07	47,02	78,37	0,03	0,90	0,73	5,97	22,85	1,47	36,91	1421,99	41,29	968,09	10,61	0,37	5,80	0,550	37,93	0,84	2,5	2,4	0,4	0,2
CS/L	L 2	2,08	0,10	0,11	0,01	0,09	0,64	46,90	78,16	0,02	1,27	1,31	8,30	13,74	2,24	17,41	15,14	23,22	888,09	14,89	0,16	0,15	0,317	43,12	1,10	3,4	0,8	0,9	0,0
	L 3B	1,61	0,10	0,10	0,01	0,08	0,64	49,12	81,87	0,03	0,85	1,10	7,16	13,92	2,00	16,09	14,74	24,08	827,76	13,09	0,27	0,13	0,407	31,02	0,85	3,7	1,7	0,8	0,1
CG/Daw	DAW 104	0,72	0,07	0,07	0,01	0,03	0,54	53,64	89,39	0,01	0,23	1,27	5,11	7,31	1,19	9,54	8,84	10,30	524,19	6,62	0,37	0,07	0,133	17,65	0,38	9,5	5,2	1,1	0,3
	DAW 102	0,23	0,05	0,06	0,00	0,02	1,18	54,59	90,98	0,01	0,12	0,79	2,01	5,30	0,72	10,16	5,86	10,78	316,60	2,75	0,09	0,06	0,114	7,61	0,12	19,0	4,1	0,8	0,1
CG/Daj	PAJ 45	0,77	0,08	0,10	0,01	0,04	2,05	52,52	87,53	0,02	0,34	0,77	4,13	8,20	1,35	11,42	15,98	15,26	387,23	7,72	0,14	0,09	0,234	16,32	0,41	5,4	1,8	0,6	0,1
	PAJ 39	0,71	0,07	0,05	0,02	0,04	3,40	51,37	85,62	0,02	0,37	0,88	3,34	7,28	1,18	14,22	33,58	18,56	443,47	6,28	0,14	0,07	0,155	17,29	0,38	6,8	2,1	0,8	0,1
	PAJ 38	0,44	0,06	0,03	0,00	0,03	1,92	54,31	90,52	0,01	0,18	0,62	2,46	14,64	0,94	11,23	6,54	10,26	359,92	4,57	0,14	0,06	0,153	10,51	0,23	7,7	3,1	0,5	0,1
	PAJ 37	1,32	0,07	0,05	0,02	0,06	5,52	45,60	76,00	0,02	0,47	0,84	5,86	9,63	1,32	14,45	22,66	16,22	388,44	8,83	0,14	0,11	0,389	22,85	0,70	3,4	1,1	0,6	0,0
CG/R	RUN 78	1,77	0,12	0,98	0,02	0,07	5,92	41,52	69,20	0,06	1,11	1,63	10,96	14,86	7,47	18,62	25,10	53,94	470,89	15,34	0,36	0,16	0,327	44,12	0,94	5,0	2,1	1,3	0,2
	RUN 77	1,11	0,13	0,75	0,01	0,04	6,43	41,09	68,48	0,03	0,56	1,45	6,00	9,42	6,73	14,72	14,61	21,88	449,90	10,06	0,84	0,11	0,287	29,12	0,59	7,1	7,7	1,2	0,7
	RUN 73	0,94	0,07	0,06	0,01	0,04	1,83	50,48	84,13	0,02	0,41	0,64	4,39	8,45	1,12	9,79	9,62	23,08	373,08	6,77	0,23	0,09	0,175	19,27	0,50	3,7	2,5	0,5	0,1
	RUN 70	1,42	0,08	0,04	0,01	0,07	3,32	45,22	75,36	0,02	0,76	1,04	5,62	10,80	1,46	12,42	11,75	18,22	428,61	9,82	0,10	0,10	0,189	34,68	0,75	4,0	0,7	0,8	0,0
	RUN 63	1,25	0,08	0,03	0,01	0,06	4,08	44,06	73,44	0,02	0,76	1,04	4,99	9,70	1,33	13,33	16,53	15,75	427,65	8,37	0,28	0,09	0,178	32,16	0,66	4,5	2,3	0,8	0,2
H/G	SG 08 20	1,22	0,07	0,01	0,01	0,05	0,44	49,42	82,37	0,03	0,35	0,44	3,55	9,35	1,05	11,08	20,69	48,34	822,31	4,00	0,12	0,08	0,189	25,57	0,65	2,0	1,0	0,2	0,0
	SG 08 18	1,23	0,08	0,01	0,01	0,05	0,51	47,69	79,48	0,03	0,41	0,50	3,46	9,78	1,05	10,58	10,62	10,01	715,14	4,16	0,06	0,05	0,202	29,73	0,65	2,2	0,5	0,3	0,0
	SG 08 14	1,07	0,08	0,01	0,00	0,05	0,68	47,97	79,95	0,02	0,34	0,45	3,09	10,36	1,18	9,91	5,88	8,93	725,50	3,92	0,09	0,05	0,225	25,11	0,56	2,3	0,8	0,3	0,0
	SG 08 09	1,55	0,09	0,01	0,01	0,07	0,50	48,39	80,65	0,04	0,46	0,58	4,25	10,42	1,04	10,32	10,19	10,96	1147,77	4,49	0,13	0,07	0,353	34,76	0,82	2,0	0,8	0,3	0,0
	SG 08 03	4,24	0,08	0,02	0,02	0,16	0,64	38,50	64,16	0,09	1,43	1,93	11,09	22,42	1,49	16,07	8,39	24,67	1169,10	9,95	0,08	0,12	0,334	94,88	2,25	2,5	0,2	1,2	0,0
T/CD	S8	0,87	0,07	0,03	0,00	0,02	1,91	53,95	89,92	0,01	0,57	1,36	1,67	5,97	0,89	5,19	2,86	13,86	358,14	6,03	0,11	0,09	0,097	16,49	0,46	8,5	1,3	1,2	0,0
	S3	1,09	0,08	0,03	0,00	0,03	1,49	51,65	86,08	0,01	1,06	0,77	2,23	7,47	0,92	6,28	5,19	16,51	295,95	8,64	0,08	0,15	0,115	21,54	0,57	3,9	0,7	0,6	0,0
	S2	0,68	0,07	0,01	0,00	0,02	0,38	57,07	95,12	0,02	0,27	1,10	1,67	6,01	0,99	6,57	3,77	16,62	1874,50	5,29	0,10	0,14	0,095	14,72	0,36	8,7	1,5	1,0	0,0
	S1	1,08	0,07	0,01	0,00	0,03	0,40	55,91	93,18	0,02	0,51	1,14	2,06	6,96	1,13	6,45	2,06	14,72	1682,22	8,20	0,07	0,11	0,129	23,83	0,57	5,7	0,7	0,9	0,0

Locations / sections	Samples	La (ppm)	Ce (ppm)	Pr (ppm)	Nd (ppm)	Sm (ppm)	Eu (ppm)	Gd (ppm)	Tb (ppm)	Dy (ppm)	Ho (ppm)	Er (ppm)	Tm (ppm)	Yb (ppm)	Lu (ppm)	Ce/Ce*	Eu/Eu*	(La/Lu)N	(La/Sm)N	(Gd/Yb)N	Pr/Pr*
CS/Do	DO6 4B	5,16	7,183	1,220	5,153	1,246	0,253	0,995	0,153	0,853	0,180	0,536	0,057	0,377	0,062	-0,34	0,07	0,95	0,60	1,60	1,14
	DO6 3	4,76	6,347	0,971	4,160	1,016	0,240	1,008	0,139	0,937	0,200	0,564	0,060	0,382	0,059	-0,32	0,12	0,92	0,68	1,60	1,09
	DO6 2A	10,16	12,225	2,133	9,619	2,104	0,473	2,193	0,336	1,949	0,421	1,216	0,125	0,819	0,143	-0,39	0,04	0,81	0,70	1,62	1,10
CS/B	B 3	8,93	16,084	2,310	10,016	1,944	0,479	1,669	0,251	1,240	0,250	0,708	0,080	0,519	0,087	-0,18	0,25	1,16	0,67	1,95	1,05
	B 99-4	7,50	10,170	1,523	6,068	1,236	0,306	1,045	0,169	0,925	0,185	0,513	0,060	0,403	0,066	-0,31	0,27	1,29	0,88	1,57	1,12
CS/L	L 2	7,09	10,129	1,655	7,366	1,391	0,345	1,274	0,166	1,047	0,190	0,529	0,063	0,378	0,066	-0,32	0,22	1,22	0,74	2,04	1,09
	L 3B	5,35	8,114	1,272	5,801	1,192	0,294	1,128	0,154	0,951	0,178	0,517	0,062	0,379	0,070	-0,28	0,19	0,87	0,65	1,80	1,06
CG/Daw	DAW 104	4,09	5,820	0,974	4,315	0,914	0,232	0,869	0,145	0,869	0,164	0,532	0,055	0,374	0,060	-0,33	0,23	0,78	0,65	1,41	1,10
	DAW 102	3,09	3,366	0,636	2,989	0,621	0,163	0,660	0,104	0,679	0,142	0,418	0,043	0,292	0,053	-0,45	0,20	0,66	0,72	1,37	1,10
CG/Daj	PAJ 45	2,35	3,424	0,519	2,336	0,392	0,122	0,501	0,084	0,418	0,081	0,216	0,031	0,208	0,037	-0,29	0,30	0,72	0,87	1,46	1,05
	PAJ 39	3,92	4,672	0,849	3,798	0,855	0,224	0,856	0,121	0,802	0,154	0,500	0,052	0,354	0,056	-0,41	0,23	0,80	0,67	1,46	1,13
	PAJ 38	2,96	3,203	0,609	2,855	0,515	0,173	0,631	0,096	0,601	0,120	0,337	0,042	0,258	0,048	-0,45	0,43	0,70	0,83	1,48	1,11
	PAJ 37	3,79	5,233	0,859	3,729	0,849	0,201	0,813	0,128	0,782	0,174	0,496	0,057	0,370	0,059	-0,33	0,14	0,73	0,65	1,33	1,11
CG/R	RUN 78	7,93	17,751	2,052	9,076	1,987	0,530	1,960	0,265	1,552	0,312	0,825	0,099	0,590	0,106	0,02	0,27	0,85	0,58	2,01	0,95
	RUN 77	5,42	10,010	1,238	5,180	1,044	0,287	1,179	0,170	0,956	0,212	0,592	0,069	0,458	0,073	-0,11	0,22	0,85	0,75	1,56	1,01
	RUN 73	4,54	6,022	1,093	4,751	1,072	0,263	0,922	0,158	1,010	0,182	0,577	0,067	0,405	0,079	-0,38	0,25	0,65	0,61	1,38	1,15
	RUN 70	6,59	6,937	1,315	5,917	1,289	0,314	1,394	0,215	1,334	0,313	0,822	0,100	0,563	0,080	-0,46	0,10	0,94	0,74	1,50	1,14
	RUN 63	10,08	9,430	2,100	9,168	2,164	0,481	2,020	0,321	1,974	0,379	1,068	0,130	0,755	0,130	-0,53	0,08	0,88	0,68	1,62	1,22
H/G	SG 08 20	6,90	7,690	1,554	7,152	1,738	0,408	1,611	0,235	1,378	0,289	0,814	0,097	0,567	0,088	-0,46	0,15	0,89	0,58	1,72	1,14
	SG 08 18	5,01	5,810	1,044	4,587	0,995	0,249	0,902	0,143	0,892	0,166	0,487	0,045	0,382	0,048	-0,41	0,24	1,18	0,73	1,43	1,14
	SG 08 14	6,57	6,605	1,337	6,045	1,388	0,312	1,363	0,187	1,143	0,219	0,624	0,074	0,430	0,070	-0,49	0,07	1,07	0,69	1,92	1,16
	SG 08 09	9,31	9,943	2,051	9,300	2,203	0,419	2,027	0,287	1,752	0,339	0,887	0,092	0,585	0,086	-0,48	-0,07	1,23	0,61	2,10	1,16
	SG 08 03	20,94	21,484	4,486	19,916	4,130	0,994	3,833	0,555	3,012	0,594	1,586	0,155	1,127	0,164	-0,49	0,18	1,44	0,74	2,06	1,19
T/CD	S8	4,93	6,643	1,149	5,678	1,071	0,331	1,029	0,120	0,838	0,171	0,367	0,042	0,266	0,044	-0,36	0,48	1,28	0,67	2,34	1,04
	S3	7,40	9,509	1,777	8,550	1,260	0,465	1,389	0,157	1,135	0,225	0,559	0,066	0,312	0,050	-0,39	0,66	1,67	0,85	2,70	1,08
	S2	4,38	4,278	0,848	4,152	0,597	0,234	0,744	0,082	0,721	0,159	0,373	0,040	0,248	0,040	-0,49	0,65	1,24	1,06	1,82	1,09
	S1	5,25	5,215	1,058	5,132	0,659	0,300	0,945	0,130	0,988	0,222	0,496	0,049	0,307	0,041	-0,49	0,79	1,44	1,16	1,86	1,10